UCRL-JC-121622
PREPRINT
CONF-950793--45

Ultra High Resolution Soft X-Ray Tomography

Waleed S. Haddad, James E. Trebes, Dennis M. Goodman, Heung-Rae Lee
Lawrence Livermore National Laboratory

Ian McNulty
Advanced Photon Source, Argonne National Laboratory

Erik H. Anderson
Lawrence Berkeley Laboratory

Andrei O. Zalensky
University of California Davis

This paper was prepared for submission to the
SPIE '95 International Society for Optical Engineering
July 9-14, 1995, San Diego, CA

July 19, 1995

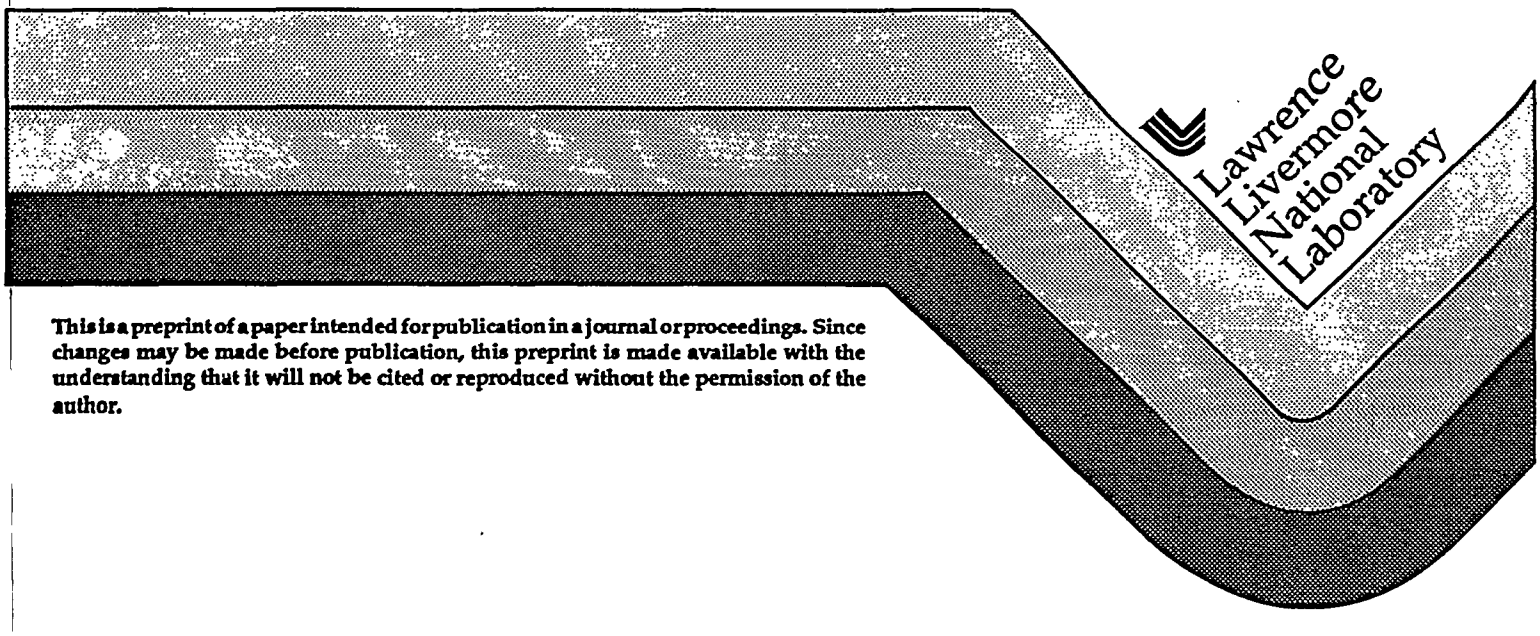

Ultra High Resolution Soft X-Ray Tomography

Waleed S. Haddad, James E. Trebes, Dennis M. Goodman, Heung-Rae Lee

University of California, Lawrence Livermore National Laboratory, Livermore, CA 94551

Ian McNulty

Advanced Photon Source, Argonne National Laboratory, Argonne, IL 60439

Erik H. Anderson

Lawrence Berkeley Laboratory, Berkeley, CA 94720

Andrei O. Zalensky

University of California Davis, Davis, CA 95616

ABSTRACT

Ultra high resolution three dimensional images of a microscopic test object were made with soft x-rays using a scanning transmission x-ray microscope. The test object consisted of two different patterns of gold bars on silicon nitride windows that were separated by ~5μm. A series of nine 2-D images of the object were recorded at angles between -50 to +55 degrees with respect to the beam axis. The projections were then combined tomographically to form a 3-D image by means of an algebraic reconstruction technique (ART) algorithm. A transverse resolution of ~1000 Å was observed. Artifacts in the reconstruction limited the overall depth resolution to ~6000 Å, however some features were clearly reconstructed with a depth resolution of ~1000 Å. A specially modified ART algorithm and a constrained conjugate gradient (CCG) code were also developed as improvements over the standard ART algorithm. Both of these methods made significant improvements in the overall depth resolution, bringing it down to ~1200 Å overall. Preliminary projection data sets were also recorded with both dry and re-hydrated human sperm cells over a similar angular range.

Keywords: x-ray microscopy, tomography, 3-D imaging, image reconstruction, optimization techniques

1. INTRODUCTION

X-ray microscopy is beginning to emerge as a viable imaging tool for microbiologists and materials scientists.[1-3] Several groups have developed x-ray microscopes of various types using synchrotron sources,[4,5] laser plasma sources,[6] and x-ray lasers.[7] All of these microscopes have produced high resolution 2-D images with soft x-rays. Transverse resolutions well below 0.1 μm have been demonstrated with scanning transmission x-ray microscopes (STXM) by Jacobsen et al.[4] and Meyer-Ilse et al.[5] There is also an increasing interest in high resolution 3-D imaging with x-rays, especially for biological specimens. X-rays are well suited to 3-D imaging for several reasons. Contrast for specific features in a specimen can be obtained by exploiting features of the x-ray absorption spectrum. Compared with electrons, x-rays offer high penetration depths, allowing sectioning of the sample to be avoided, and they cause less radiation damage for images of equal contrast.[8] There are however no x-ray optics having sufficiently high numerical aperture (NA) to achieve resolution in depth that is comparable with the transverse resolution. Currently the best x-ray zone plates have a NA < 0.1 for radiation in the water window.[9] This means that the ratio of depth resolution to transverse resolution $\partial l/\partial t \approx 2/NA = 20$ for present state-of-the-art zone plates.

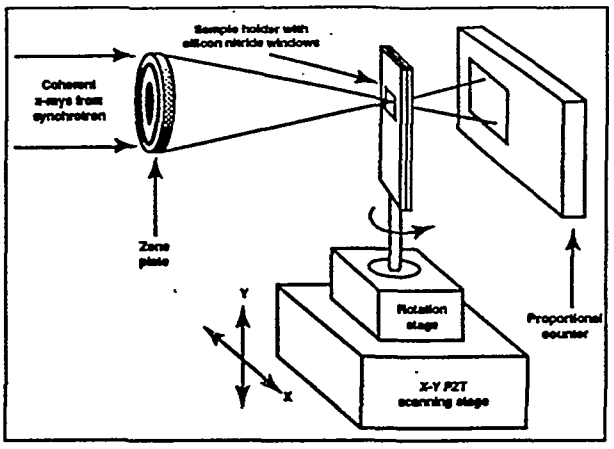

Fig. 1. Sketch of the scanning transmission x-ray microscope (STXM) with the rotatable sample holder.

It is possible to improve the depth resolution by recording several views of the object over a large angular range. If each of the views is taken with a low NA optic such that the longitudinal extent of the object is less than the depth resolution of the imaging system, then each view will be a 2-D projection of the object. If, in addition, the images are recorded incoherently, as is the case with the STXM, then diffraction is not a factor. A 3-D image of the object can then be formed by combining the set of 2-D projections tomographically. The quality of the reconstructed image will depend on the quality of the projection data, the number of projections and the angular range over which they are taken. We have implemented this approach in conjunction with the STXM on the X1A beamline at the National Synchrotron Light Source (NSLS) in Brookhaven National Laboratory. The STXM forms high resolution 2-D images by scanning a sample through a focused beam of x-rays in a raster pattern orthogonal to the beam axis.[4] We modified the scanning stage of the STXM to include a rotational stage so that the images of a specimen could be taken over a range of angles. Figure 1 is a sketch of the STXM with the rotatable sample holder. We used this modified STXM to make a high resolution 3-D image of an artificial test object. The resulting 3-D image shows an improvement in resolution of nearly an order of magnitude compared with existing x-ray tomographic techniques. Detailed descriptions of this work have been published elsewhere.[10, 11] We have also begun extending these techniques to biological specimens. Currently, we are developing sample preparations for imaging single cells in 3-D, and some preliminary multi-view data have been obtained with human sperm cells.

2. IMAGING OF THE TEST OBJECT

The test object consisted of two unique patterns of 650 Å thick gold bars written onto silicon nitride windows which were separated by ~5μm. The two patterns were designed to be simple yet contain a range of features of various sizes including gaps and angles other that 90 degrees. Each pattern was comprised of bar features in the size range between 1000 Å and 5000 Å, and occupied a 2 μm x 2 μm region on the window. The overall dimensions of the test object were approximately 2 μm x 2 μm x 5 μm. For good 3-D image formation, it was necessary that the object be partially transmissive while providing good contrast. As a result, the thickness of 650 Å was chosen for the gold patterns based on computer simulations. A sketch of the test object is shown in Fig. 2. The two gold patterns in the figure are labeled A and B for future reference. The rectangular frame at the top of pattern A was incorporated into the test object as an alignment diagnostic. This frame was imaged along with the object from each viewing angle and was used as an aid in aligning the projections, however, the portion of each 2-D image containing the frame was not included in the 3-D reconstruction. When forming images with the STXM, it is necessary to filter out higher order foci of the zone plate by passing the beam after the zone plate through an order sorting aperture (OSA). In order to allow clearance for rotation of the sample the OSA (not shown in the figure) was incorporated into the test object. The OSA was a 7000 Å thick gold mask with a 10 by 15 μm aperture centered over pattern A.

The x-ray source at X1A is an undulator that produces a high flux of tunable coherent soft x-rays in the energy range of 250 to 800 eV.[12] For these experiments the beamline was operated at a wavelength of 36 Å and a spectral width of 0.5%. The x-rays were focused onto the test object by a zone plate with a finest zone width of 600 Å. This produces a near diffraction limited spot of about 732 Å.[13] Scans were made with a step size of 250 Å, thus oversampling by approximately 3:1.

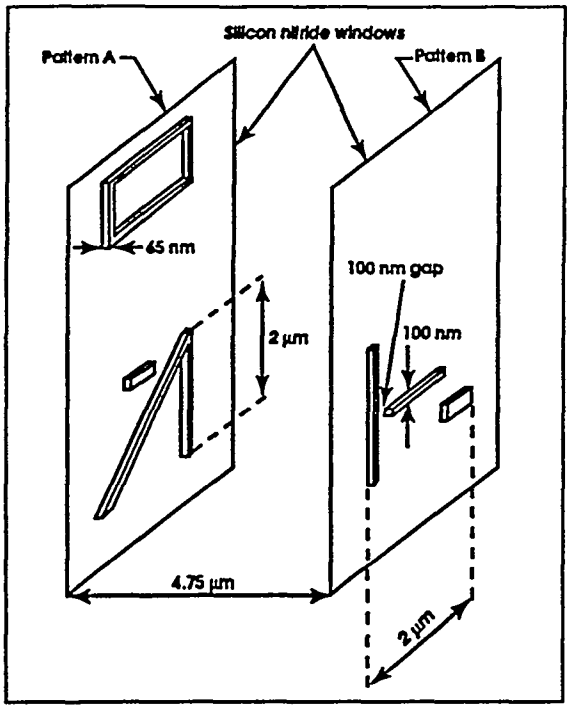

Fig. 2. Sketch of the 3-D microscopic test object. The two gold patterns were written using electron beam lithography.

Physical limitations of the instrument allowed only a small number of projection images to be taken and restricted the angular range over which projections could be recorded. For this experiment, 9 projection images were recorded at angles between -50 and +55 degrees. The combination of limited viewing angle and few projections results in a challenging image reconstruction problem. In cases such as this, the amount of information in the projections is much less than that needed to straight forwardly reconstruct the image; ie., the reconstruction problem is ill-posed and it is necessary to use an iterative optimization technique for reconstruction. We used an algebraic reconstruction technique (ART) code to form a volumetric data set of the test object from the set of 2-D projections.[14, 15] Prior to reconstruction, the raw projection data were aligned, corrected for irregularities and the logarithm of the brightness of each projection was taken in order to make it a linear function of material thickness.

We observed a transverse resolution of ~750 Å in the 2-D images which can be inferred from feature edges and the resolution of the 1000 Å gap in pattern B (see Fig. 2). Artifacts in the 3-D reconstruction due to noise in the 2-D projections, uncertainty in the measurements of the projection angles, misalignment of the projections, the limited angular range over which the projections are recorded, the limited number of projections and fundamental limits of the reconstruction technique limited the depth resolution while producing a loss in transverse resolution compared with the 2-D images. As a result, the transverse resolution in the 3-D reconstruction was close to 1000 Å. The overall depth resolution was limited to about 6000 Å, however some features were clearly resolved at 1000 Å in depth. Figure 3 is a series of 2-D rendered images of the 3-D reconstruction. Most noteworthy are the views presented for angles of rotation about the horizontal axis since 2-D projections from similar angles were not recorded. Clearly visible are the two patterns shown in Fig. 2. The effects of the reconstruction artifacts can be seen in Fig. 3. The only feature suffering from significant distortion is the horizontal bar of pattern B, which has ballooned to about 6000 Å full width at half maximum in the depth dimension. This is a result of the limited angular range over which projections were taken and the inability of the ART algorithm to confine the mass of the feature in the depth direction with the limited data set.

3. PROGRESS TOWARDS IMPROVED IMAGE RECONSTRUCTION

Recently, we have been developing improved image reconstruction techniques to better handle the problems of limited number of projections and limited angular range of the projections. Two methods have arisen. The first is a constrained conjugate gradient (CCG) optimizer applied to tomography, and the second is a modification of the ART code mentioned above. A detailed description of these algorithms is beyond the scope of this paper, however the CCG algorithm has been previously applied to other problems, and is published elsewhere.[16, 17]

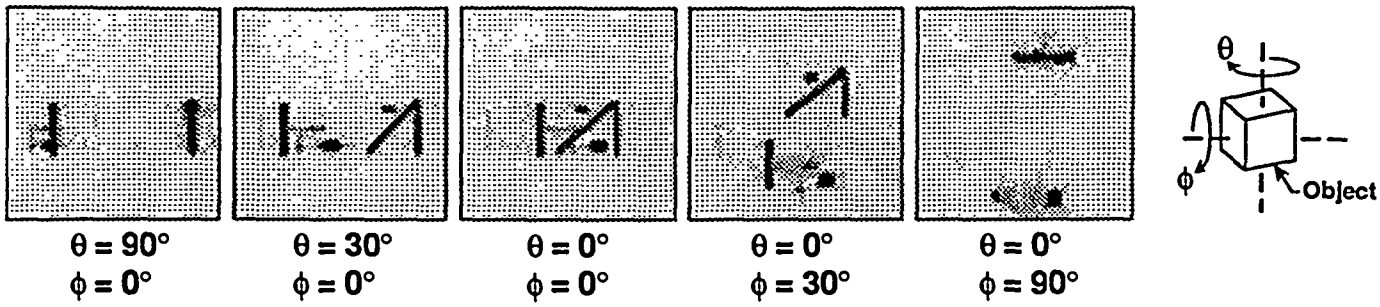

Fig. 3. Views of the 3-D reconstruction of the test object at various orientations. Each image in the figure is a rendered perspective, not a simple projection, of the object.

We will hereupon refer to the special modified ART as SPART. Standard ART works well within the first few (up to ~100) iterations, but bogs down after that because, in general, the rate of convergence diminishes with the number of iterations. If the data is noiseless, ART continues to converge with more iterations, albeit so slowly that improvements in the reconstruction are nearly undetectable. The SPART code attempts to deal with this problem through the use of prior knowledge that the projection data were limited in range. SPART uses the knowledge that at any point in the iterative reconstruction process, the reconstructed image is always blurred in the depth dimension; the same blurring that is visible in the reconstructions of Fig. 3. The SPART code attempts to "push" the reconstruction process towards better convergence by a compression in the depth dimension of the reconstructed image on every iteration. This compression must be done in small increments after each iteration so as to avoid instabilities. The current version of the SPART code accomplishes this by calculating the 90 degree angle projection of the image, and then backprojecting it into the image after each iteration. This causes a gentle sharpening of the image in the depth dimension after every iteration. The process is stopped when the mean square difference between the real projection data and the calculated projections of the current reconstruction is less than a predetermined value.

All the reconstruction techniques described herein form 3-D images as a series of 2-D slices which are normal to the axis about which the sample was rotated. It is clear from the images in Fig. 3 that the slices containing the features which are most difficult to reconstruct pass through the center of the test object and contain the horizontal bar of pattern B. We therefore choose one of these slices as a gauge of our reconstruction techniques, and compare them by forming images of only this one slice using the various reconstruction techniques, and comparing them with each other and with an ideal model of the slice. These images are shown in Fig. 4. Both the CCG and SPART reconstruction techniques produce images with marked improvement over the standard ART reconstruction. Both of these techniques improve the *overall* depth resolution in the images of the test pattern from 6000 Å to approximately 1200 Å, making the depth resolution truly comparable to the transverse resolution for this imaging technique.

Fig. 4. Comparison of the three tomographic image reconstruction techniques. The figure shows four 2-D images of a central slice of the test object. a) ideal model image, b) standard ART reconstruction from 9 the projections, c) CCG reconstruction, d) SPART reconstruction.

4. FIRST MULTI-VIEW DATA OF SINGLE CELLS

We have been focusing on 3-D imaging of sperm cells for various reasons. They are of great interest to molecular and cell biologists because of their importance in the reproductive process. The geometric structure of the DNA within the cell is not well known, and it has been suggested that its exact geometry may play a critical role in fertilization. Samples of human sperm cells were prepared with gold labeling and chemically induced to swell in size by approximately a factor of 6. Two sets of samples were prepared, one with telomere specific probes, and the other with centromere specific probes. Droplets of solution containing prepared cells were placed onto silicon nitride windows having OSAs similar to the one described above for the test pattern, and allowed to dry. Only the windows having one or two cells within the OSA were selected for use in the experiment. Multi-view data sets of several of these dry samples were taken.

Ultimately, the goal is to be able to image hydrated specimens as close to their living state as possible. In a first step towards this goal, we prepared some wet sperm samples by re-hydration. It is necessary to have a sample package which can hold a wet cell specimen, carry an OSA and allow the entire package to be rotated so that images of the cell could be recorded over a wide range of angles. These wet cell packages were prepared by taking the same dry preparations described above, and cementing another silicon nitride window onto the window carrying the OSA and the dried sperm cell in such a way as to sandwich the cell between the two windows. Epoxy was used to fasten the two windows together and to form a seal on two parallel sides of the window sandwich. Just prior to imaging, one open end of the sample packages were dipped into water. Capillary forces drew a small amount of water upwards, filling the gap between the windows and re-hydrating the specimens. The remaining open ends of the sample packages were then sealed with epoxy, capturing a several micron thick water layer between the windows. Multi-view data sets of two of these re-hydrated samples were recorded. Representative images from both the dry and re-hydrated data sets are presented in Fig. 5.

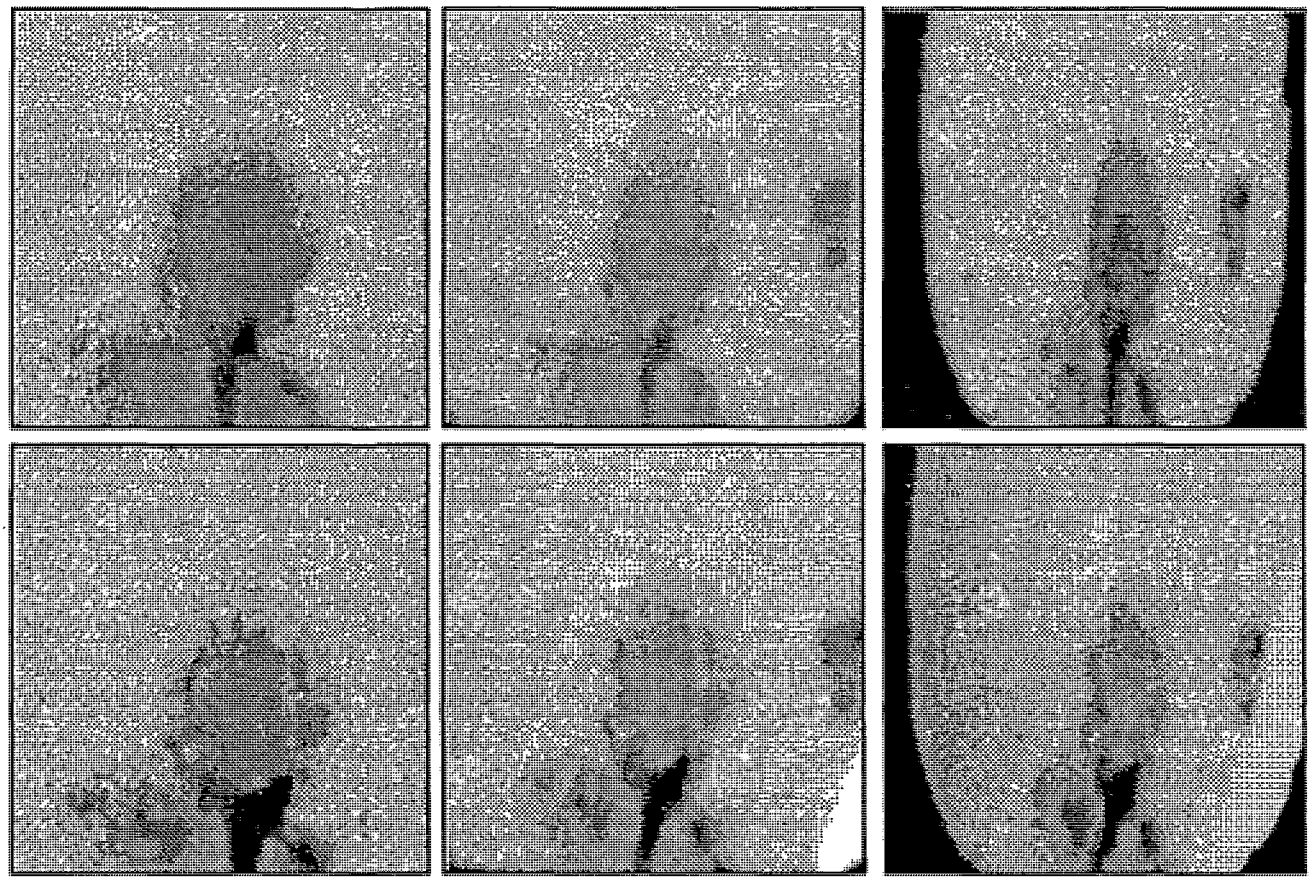

Fig. 5. Images of gold labeled human sperm cells taken at different angles. This sample had two overlapped cells within the OSA. The top three panels are projections taken of the dried sample. The lower three panels show the same three projections of the same sample after re-hydration. The edge of an air bubble is visible as a bright region in the lower right corner of the bottom row of images.

5. SUMMARY

Ultra high resolution tomography with a scanning transmission x-ray microscope has been demonstrated. A 3-D image of a microscopic test object was produced with an algebraic reconstruction technique from nine 2-D soft x-ray micrographs. Two improved reconstruction techniques were also developed to better handle the problem of reconstruction of the 3-D image from limited projection data. The 3-D reconstructions have depth resolution comparable to the high transverse resolution of the 2-D images, and to our knowledge, are the highest resolution x-ray tomographic images to date.[18, 19] Preliminary multi-view data sets of both dry and re-hydrated, gold labeled human sperm cells were also recorded.

6. ACKNOWLEDGMENTS

We thank Rod Balhorn for his crucial influence and involvement in the biological specimen preparations, Stephen Azevedo and Erik Johansson for their work on the CCG tomography code, the IBM Research Staff for their involvement in fabricating the test patterns, and the staff at the X1A beamline at NSLS for their support.

This work was performed under the auspices of the U.S. Department of Energy under contracts W-7405-ENG-48* and W-31-109-ENG-38. The lithography work was supported by the Director, Office of Energy Research, Office of Basic Energy Science, U.S. Department of Energy under contract No. DE-AC03-76SF00098

7. REFERENCES

1. M. R. Howells, J. Kirz, and D. Sayre, Sci. Am. 264, 88, (1991)
2. For example see: *X-Ray Microscopy*, G. Schmahl and D. Rudolph, Eds. (Springer-Verlag, Berlin, 1984); *X-Ray Microscopy II*, D. Sayre, M. Howells, J. Kirz, H. M. Rarback, Eds. (Springer-Verlag, Berlin, 1988)
3. Also see: *X-Ray Microscopy III*, A. Michette, G. Morrison, C. Buckley, Eds. (Springer-Verlag, Berlin, 1991)
4. C. Jacobsen et al., Opt. Commun. 86, 351 (1991)
5. W. Meyer-Ilse et al., in (3), pp. 284-289.
6. T. Tomie et al., *Science* 252, 691 (1991)
7. L. B. Da Silva et al., *Science* 258, 269 (1992)
8. D. Sayre, J. Kirz, R. Feder, D. M. Kim and E. Spiller, Science 196, 1339 (1977)
9. E. H. Anderson and D. Kern, in (3), pp. 75-78.
10. W. S. Haddad et al., *Science* 266, 1213 (1994)
11. I. McNulty, W. S. Haddad, J. E. Trebes, E. H. Anderson, *Rev. Sci. Instrum.* 66, 1431 (1995)
12. H. Rarback et al., *J. X-ray Sci. Tech.* 2, 274 (1990)
13. C. Jacobsen, J. Kirz and S. Williams, *Ultramicroscopy* 47, 55-79 (1992)
14. A. C. Kak and M. Slaney, Principles *of Computerized Tomographic Imaging* (IEEE Press, New York, 1988) chap. 3.
15. D. Verhoeven, Appl. Opt. 32, 3736 (1993)
16 D. M. Goodman, E. M. Johansson, T. W. Lawrence, *Multivariate Analysis: Future Directions* (Elsivier Science Publishers, Amsterdam, 1993)
17 D. M. Goodman, J. Kolman, S. G. Azevedo, "Image Reconstruction with Optimal Constraints", *Engineering Research, Development and Technology Thrust Area Report*, UCRL 53868-94, 8-1 (1995)
18. B. P. Flannery, H. W. Deckman, W. G. Roberge and K. L. D'Amico, *Science* 237, 1439 (1987)
19. J. H. Kinney et al., *Science* 260, 789 (1993)

---

* by Lawrence Livermore National Laboratory